nanomaterials

MDPI

Article

Synthesis and HRTEM Investigation of $EuRbFe_4As_4$ Superconductor

Alena Yu. Degtyarenko [1,*], Igor A. Karateev [2], Alexey V. Ovcharov [2], Vladimir A. Vlasenko [1] and Kirill S. Pervakov [1]

[1] V.L. Ginzburg Centre for High-Temperature Superconductivity and Quantum Materials, P.N. Lebedev Physical Institute of the Russian Academy of Sciences, 53, Leninsky Ave., Moscow 119991, Russia
[2] National Research Centre "Kurchatov Institute", 1, Kurchatov Sq, Moscow 123182, Russia
* Correspondence: degtyarenkoayu@lebedev.ru

Abstract: In the stoichiometric iron-based superconductor $EuRbFe_4As_4$, superconductivity coexists with a long-range magnetic ordering in Eu layers. Using high-resolution transmission electron microscopy (HRTEM), we observed an atomic structure of as-grown $EuRbFe_4As_4$ crystals. HRTEM shows that crystals have two-dimensional intrinsic nanoinclusions established to be the $RbFe_2As_2$ (122) phase with a volume fraction of ~5.6%. In contrast with the $CaKFe_4As_4$ compound, similar inclusions are not superconducting down to 2 K, and no second magnetization peak was observed in the magnetization measurements at low temperature with B ∥ ab. We show that the non-superconducting 122 phase nanoinclusions could act as 2D pinning centers.

Keywords: iron-based superconductors; IBS; 1144; microstructure; 2D pinning centers; HRTEM; magnetic superconductors

check for updates

Citation: Degtyarenko, A.Y.; Karateev, I.A.; Ovcharov, A.V.; Vlasenko, V.A.; Pervakov, K.S. Synthesis and HRTEM Investigation of $EuRbFe_4As_4$ Superconductor. *Nanomaterials* **2022**, *12*, 3801. https://doi.org/10.3390/nano12213801

Academic Editor: Yassine Slimani

Received: 3 October 2022
Accepted: 26 October 2022
Published: 28 October 2022

Publisher's Note: MDPI stays neutral with regard to jurisdictional claims in published maps and institutional affiliations.

Copyright: © 2022 by the authors. Licensee MDPI, Basel, Switzerland. This article is an open access article distributed under the terms and conditions of the Creative Commons Attribution (CC BY) license (https://creativecommons.org/licenses/by/4.0/).

1. Introduction

Nowadays, scientists all over the world are actively researching so-called magnetic superconductors in which superconductivity and ferromagnetism coexist simultaneously, which previously seemed completely impossible. Up to the present time, superconducting transition temperatures in magnetic superconductors were quite low and did not exceed 10 K [1–3]. With the 2008 discovery of iron-based superconductors where superconductivity exists in the FeAs planes, critical temperatures increased significantly from 26 up to 57 K [4–6].

A novel iron-based superconducting (SC) family, known as 1144-type, was discovered in 2016 [7,8]. The stoichiometric $AeAFe_4As_4$ compounds (Ae = Ca, Sr, Ba, Eu and A = K, Rb, Cs) with space symmetry group P4/mmm are formed by two alternating structures, $AeFe_2As_2$ and AFe_2As_2, see Figure 1a,b. Unlike the Ba-122 [9,10] system, the 1144-type does not form solid solutions because of the large difference in ionic radii between alkaline (A) and alkali-earth (Ae) atoms but fills the crystallographic positions alternately between the FeAs planes. Among the 1144 iron-based superconductors, the europium-containing compounds $AEuFe_4As_4$ (A = Rb, Cs) are the materials with coexistence between superconductivity and magnetism [11], with a magnetic transition temperature lower than the superconducting one (T_c = 35–37 K). Magnetic ordering of europium in the $EuRbFe_4As_4$ compound occurs at T_m~15 K and has helical structure [12]. Despite the magnetic structure and the superconducting condensate being spatially separated from each other [13,14], magnetic interaction occurs between the Eu layers by superconducting ones. Such a pancake of alternating superconducting FeAs layers and magnetic Eu atoms is a natural analog of the layered superconductor–magnet (SC–M) heterostructure, but with self-assembly at the nanoscale, it opens up the prospects of Eu spin manipulation for electronics.

The value of the upper critical magnetic field H_{c2} in $EuRbFe_4As_4$ reaches 100 T [15]. Among other things, the $EuRbFe_4As_4$ compound has a surprisingly low superconducting

anisotropy of ~1.7 at low temperatures. The coherence lengths ξ_{ab} (in-plane) and ξ_c (out-of-plane) are 1.4 nm and 0.92 nm, respectively [16].

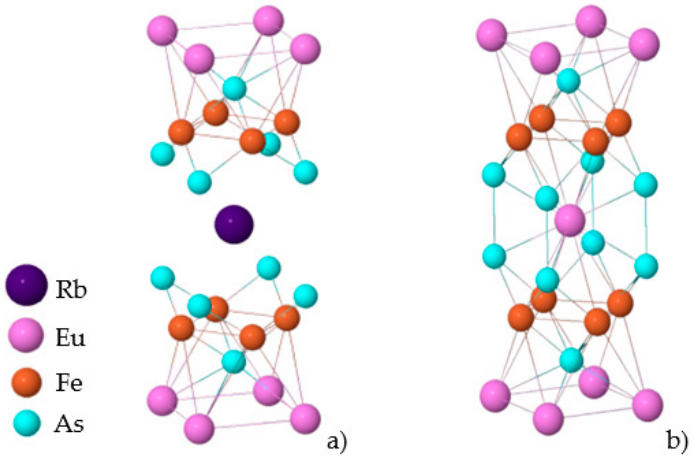


Figure 1. Crystal structure models of 1144 (**a**) and 122 (**b**).

The growth of pure 1144 single crystals is not an easy task because of competition between the 1144 and the 122 phases during crystallization. While heating the initial components at temperature about T = 800 °C, two compounds, Ae-122 and A-122, are formed with the subsequent start of the 1144 phase formation at 900 °C [17]. According to the model given in [18], two conditions are necessary for the successful phase formation: lattice parameter matching and charge transfer between the blocks. For the 1144 phases, every fluctuation in synthesis leads to structural instabilities; therefore, obtaining a homogeneous 1144 phase is quite difficult due to the presence of a small fraction of 122 inclusions. During the $EuRbFe_4As_4$ synthesis, the appearance of both $EuFe_2As_2$ (Eu-122) and $RbFe_2As_2$ (Rb-122) impurity phases is possible. The $EuFe_2As_2$ compound has two phase transitions at about 190 K and 20 K [19]. The first one at T_0 = 190 K is due to a spin density wave (SDW) along with a crystallographic phase transition from the tetragonal phase (I4/mmm) to an orthorhombic phase (Fmmm) and the AFM transition in the iron sublattice [20]. The phase transition at 20 K is caused by the AFM ordering of the Eu^{2+} moments. In Rb-122, temperature dependence of the resistivity behavior is the same as for a normal metal. The magnetic susceptibility, however, shows the broad peak around 80 K [21]. This feature has been assumed to be a disordered magnetism [22] or an orbital selective Mott insulator transition in the normal state [23] similar to KFe_2As_2.

Currently, the $CaKFe_4As_4$ compound microstructure has been studied in detail [24,25] with the use of HRTEM, where two-dimensional superconducting intergrowths of (Ca, K)Fe_2As_2 compatible with the appearance of second magnetization peak were found. However, there are no $EuRbFe_4As_4$ microstructure investigations explaining the vortex pinning properties. Thus, we study the single crystals of $EuRbFe_4As_4$ by HRTEM to find the correlation between the structure defects and SC properties.

2. Materials and Methods

The $EuRbFe_4As_4$ single crystals were prepared by the "self-flux" method in an RbAs flux. The preparation was carried out in a glove box in an argon atmosphere. High-purity metals Eu (Lanhit, 99.95%), Fe (ABCR, 99.98%), Rb (NZRM, 99.99%), and As (Lanhit, 99.9999%) were used to produce precursors EuAs, Fe_2As, and RbAs. An excess of Rb was used to compensate Rb evaporation, and prolonged synthesis was performed to obtain up to the 100% of the RbAs phase. The obtained precursors were mixed in the required stoichiometric ratio with an addition of flux [RbAs] by the following reaction (1):

$$EuRbFe_4As_4 = EuAs + 2Fe_2As + RbAs + 2[RbAs] \quad (1)$$

Then, the reactants were placed in an alumina crucible, welded in a niobium container under residual argon pressure of 0.2 atm (Figure 2a,b), and subjected to a multi-stage heat treatment similar to our previous works with a FeAs flux [26,27]. After the synthesis, $EuRbFe_4As_4$ (EuRb-1144) crystals were collected from the crucible in an argon glove box and stored in it to avoid contact of the grown crystals with the air atmosphere and possible degradation. In our previous work [26], we showed the as-grown EuRb-1144 single crystals to be degraded after air exposure. The cleaved $EuRbFe_4As_4$ single crystals with a smooth and shiny surface are shown in Figure 2c.

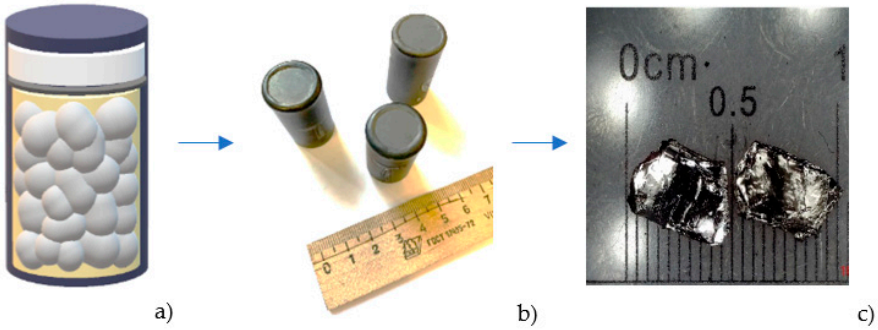


Figure 2. $EuRbFe_4As_4$ single crystals obtaining scheme: (**a**) reactants embedded in an alumina crucible and (**b**) welded in a niobium container, (**c**) $EuRbFe_4As_4$ single crystals.

Temperature dependences of the AC magnetic susceptibility and magnetic moment measurements in B || ab and B || c orientations up to 9 T were measured with a PPMS-9 Quantum Design system (San Diego, CA, USA). The AC magnetic susceptibility measurements were carried out with H_{ac} = 5 Oe. XRD (X-Ray diffraction) analysis was conducted with Rigaku Smartlab (Osaka, Japan) (in-plane $2\theta/\omega$ scan) at Cu $K\alpha$ with Ge-monochromator (220) × 2. The diffraction pattern was obtained in the range of 2θ angles 5–60°.

The SEM (scanning electron microscopy) investigations were performed with a Helios NanoLab 600i scanning electron-ion microscope (Thermo Fisher Scientific, Waltham, MA, USA) equipped with EDS (energy-dispersive spectroscopy) analyzer (Ametek, Berwyn, PA, USA), Pt and W gas injection systems (GIS), and an OmniProbe 200 micromanipulator (Oxford Instruments, Abingdon, Oxfordshire, UK). For HRTEM studies, samples were prepared by a focused ion beam (FIB) technique. The samples were studied using a Titan 80–300 (Thermo Fisher Scientific, MA, USA) transmission (scanning) electron microscope with accelerating voltage of 300 kV with a beam probe size in the STEM mode of 0.8 A. The microscope is equipped with a sample spherical aberration corrector (Cs-corrector), a high-angle annular dark-field detector (HAADF), an X-Ray microanalysis system (Ametek (EDAX), PA, USA), and a characteristic electron energy loss spectroscopy system (Gatan (Ametek), Pleasanton, CA, USA). Image post-processing was performed using Digital Micrograph (Gatan (Ametek), CA, USA) and Tecnai Imaging and Analysis (Thermo Fisher Scientific, MA, USA) software.

3. Results and Discussion

Before HRTEM investigations, we selected a sample with a negligible feature around 19 K in magnetic measurements associated with $EuFe_2As_2$ phase inclusions. To prevent the delamination of the single crystals, all necessary manipulations were performed in an argon glove box using parafilm or vacuum desiccator. Figure 3a shows temperature dependence of the AC susceptibility of $EuRbFe_4As_4$ single crystal selected for TEM investigations along the ab plane. Using the onset criteria, we found the critical temperature of the superconducting transition T_c (T_c = 36 K). The T_c value is similar to one presented in other papers [26,28]. The Eu^{2+} magnetic ordering of EuRb-1144 feature at $T_m \approx 15$ K is shown in Figure 3a. In Figure 3b, one can see the XRD pattern of the EuRb-1144 crystal by in-plane $2\theta/\omega$ scan. The pattern contains only reflections with *(00l)* orientation that

demonstrate the monocrystallinity of the sample. In addition, a small amount of Rb-122 (see Rb-122 *(002)* and *(004)* reflections) and Eu-122 (see Eu-122 *(002)* and *(004)* reflections) phases were detected.

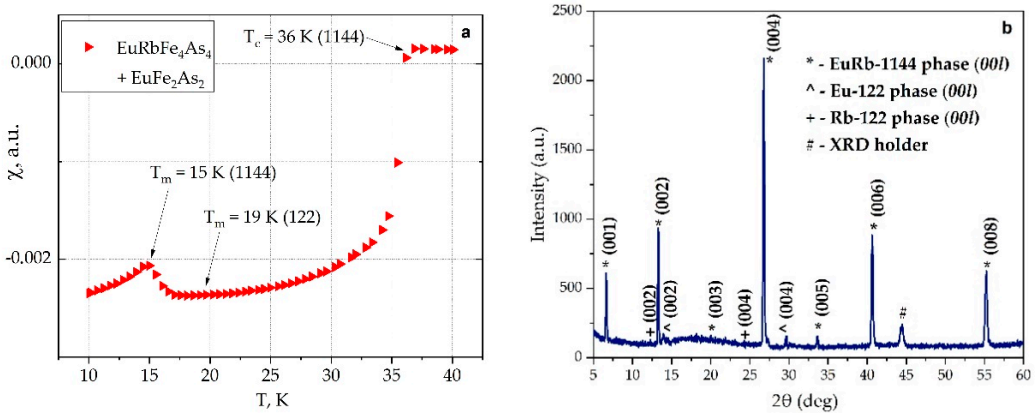


Figure 3. (**a**) Temperature dependence of the AC magnetic susceptibility of the EuRb-1144 sample ($T_m \approx 15$ K, $T_c \approx 36$ K) and non-superconducting trace inclusions of the Eu−122 phase ($T_m \approx 19$ K); (**b**) XRD pattern of the EuRb-1144 crystal.

Then, part of the selected sample with a minimum inclusion of 122 phase was loaded into the sample exchange chamber, evacuated, and transferred to the microscope chamber, and elemental mapping of the surface of the $EuRbFe_4As_4$ single crystal was carried out by scanning electron microscopy, see Figure 4.

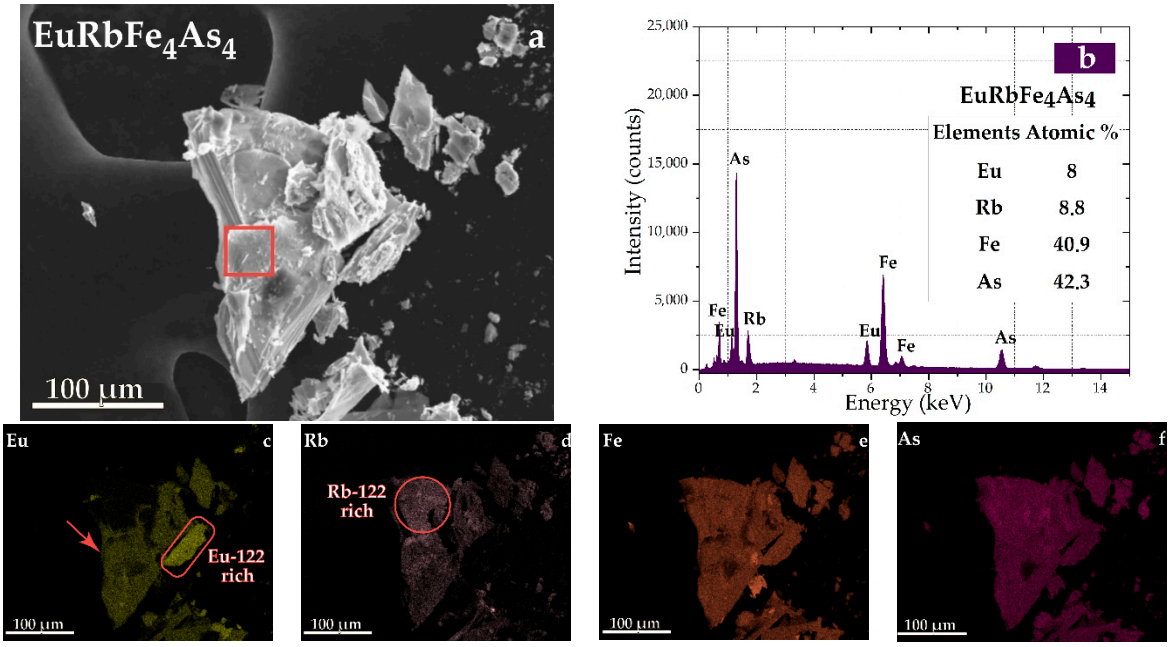


Figure 4. (**a**) SEM images of the $EuRbFe_4As_4$ single crystal in mapping mode; (**b**) EDS analysis spectra of the $EuRbFe_4As_4$; and maps of: (**c**) Rb; (**d**) Eu; (**e**) Fe; (**f**) As.

An energy dispersive (EDS) analysis confirms the presence of some areas with Eu-122 and Rb-122 phase predomination in the EuRb-1144 sample as shown in Figure 4c. We chose the single crystal part indicated by the red arrow (Figure 4c) for the lamella cutting, which had a required stoichiometric composition $EuRbFe_4As_4$ (Figure 4b). The lamella was cut along the c axis and investigated by a transmission electron microscope.

Figure 5a,c present the HAADF STEM images of $EuRbFe_4As_4$ single crystal microstructures along the c plane. In the bulk of the EuRb-1144 sample, dark stripes of inclusions are observed, which are located along the ab plane. HAADF STEM images have Z-contrast; therefore, the dark stripes correspond to the absence of Eu atoms. A high-resolution image (Figure 5c) of defect and the corresponding intensity profile (Figure 5d) confirm this. The lattice parameters for the structural 122 defects were determined from the profile and found to be a, b = 0.38 nm, c = 1.45 nm, which is in a good agreement with the Rb-122 crystal structure data. The atomic lattice period for the EuRb-1144 phase was determined from the electron diffraction pattern, Figure 5b. The lattice parameter of EuRb-1144 is c = 1.319 nm and a, b = 0.388 nm, which complies well with the reference data [29].

The length of two-dimensional nanodefects along the ab plane is more than 200 nm, and the volume of inclusions is about 5.6% from the selected area 200×200 nm^2 (Figure 5a). It should be noted that our sample was grown in the RbAs flux; thus, the Rb-122 intergrowths should dominate. Moreover, the electron diffraction pattern from the inclusion of Rb-122 cannot be obtained due to the small area. In the case of FeAs flux growth, the $EuFe_2As_2$ inclusions might be more frequent. Iyo et al. experimentally show a second magnetization peak (SMP) in CaK-1144 samples in the applied external magnetic field along ab direction [24]. According to the proposed model, the SMP was associated with superconducting nanoscale (Ca, K)Fe_2As_2 intergrowths inherent to a CaK-1144 single crystal along the ab plane. In our $EuRbFe_4As_4$ single crystal, the directly observed $RbFe_2As_2$ single nanolayers should not be superconducting down to 2.1–2.6 K [30,31]. The possible two-dimensional inclusions of $EuFe_2As_2$ (it was registered by magnetic susceptibility and XRD measurements) are well-known to be non-superconducting [32]. Thus, according to the abovementioned qualitative model, there should not be an SMP on the magnetic irreversibility loops above 2 K. To verify this statement, we measured the magnetic irreversibility loops at 2 and 4 K in fields up to 9 T in parallel and perpendicular field orientation to the ab plane.

In Figure 6, one can find the magnetic irreversibility loops of investigated $EuRbFe_4As_4$ single crystal at T = 2 and 4 K with the B ∥ ab and B ∥ c, respectively. It is clearly seen that there are not any features in all cases with the exception of the kink of the loops attributed to magnetic nanoinclusions (Eu-122, iron atoms). The enlarged central part of the hysteresis loops at T = 2 K for both field directions presented in Figure 6b show a clear diamagnetic signal with increasing the magnetic field from B = 0, which point to domination of the superconducting signal. As shown recently, the loop width (ΔM) value is weakly depend on magnetic impurities and on helical magnetic ordering in EuRb-1144 down to low temperatures [16,26]. Therefore, we may use Bean's critical state model [33] without taking into account the contribution of the magnetic inclusions in order to investigate J_c curves behaviour. We calculated J_c/J_c max(B) curves at T = 2 K (much lower than the magnetic transition), where $J_c \sim \Delta M$, and plotted in Figure 6c. One can clearly see the monotonous J_c(B) dependence without any second magnetization peak in both field orientations. Similar to the $CaKFe_4As_4$ (CaK-1144) which shows significant SMP in B ∥ ab field orientation, in the EuRb-1144 system we found 122 phase monolayered nanoscale intergrowths (Rb-122) in the volume of the EuRb-1144 superconductor. However, the Rb-122 nanolayers seem to be non-superconducting down to 2 K and have no visible second magnetization peak appearance on the magnetic irreversibility loops. This experimentally confirms the assumption that the SMP was attributed to SC nanoscale intergrowths along the crystallographic ab plane. In our previous paper [26], we claimed the two-dimensional pinning predominance in the $EuRbFe_4As_4$ system with B ∥ ab. The direct HRTEM observation of Rb-122 nanoscale intergrowths support our suggestion about the predominance of two-dimensional pinning of the Abrikosov vortices in this system.

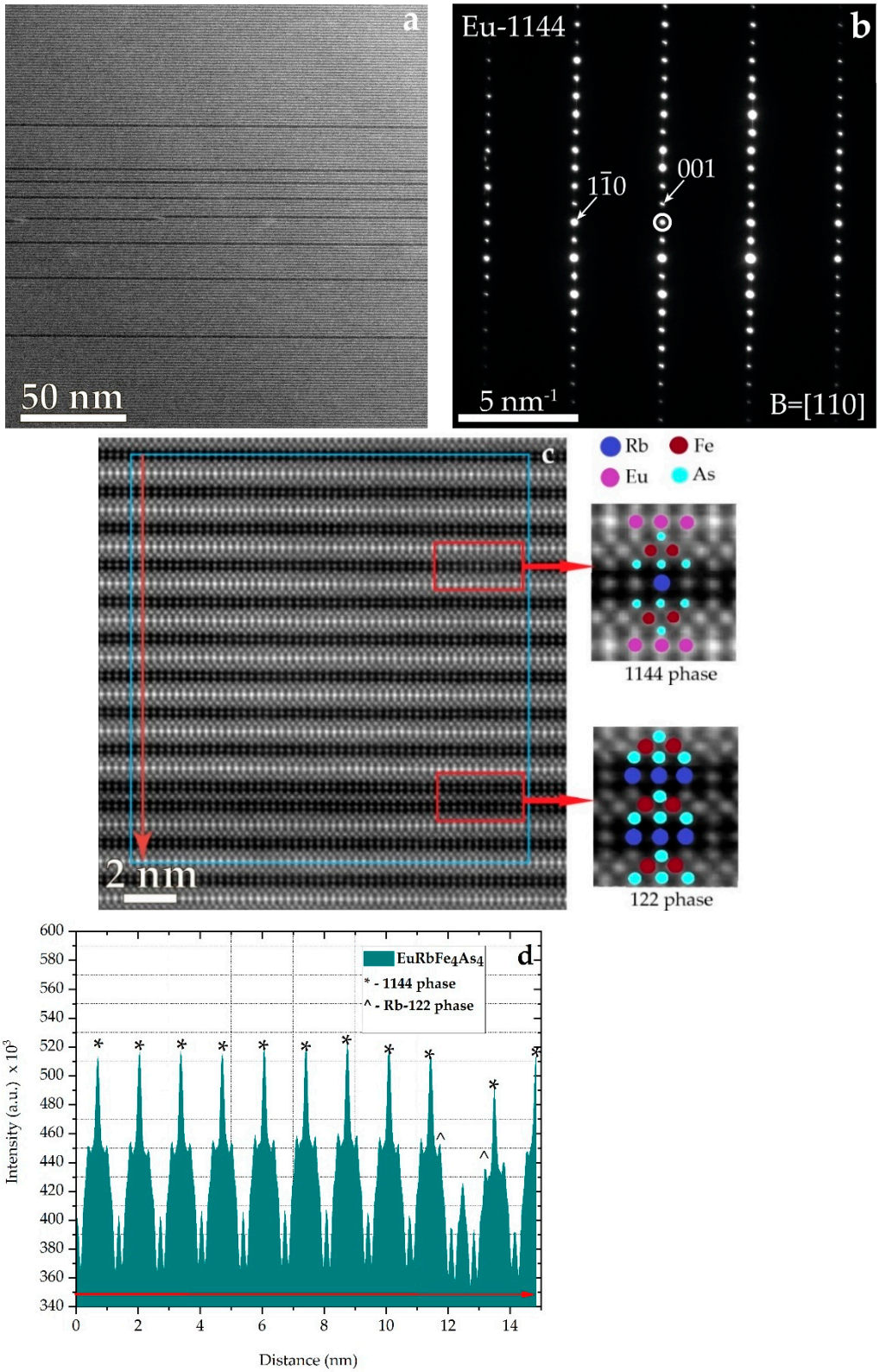


Figure 5. HAADF STEM images (**a**,**c**) of microstructures of the $EuRbFe_4As_4$ with black stripes of two-dimensional defects of the $RbFe_2As_2$, selected area diffraction pattern from EuRb−1144 phase (**b**); intensity profile (**d**); from the selected blue area (**c**).

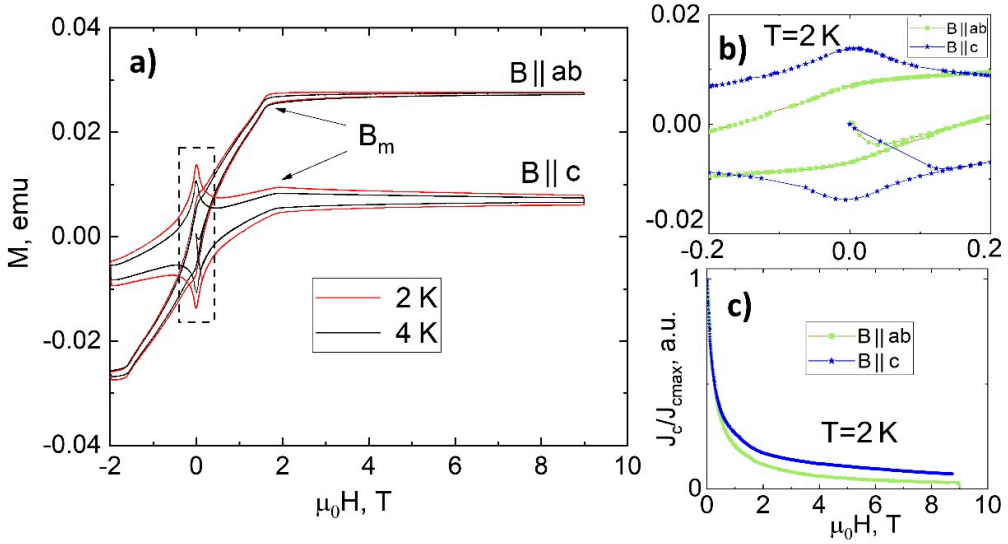


Figure 6. (**a**) Isothermal magnetization hysteresis data for EuRb−1144 as a function of magnetic field (up to 9 T) with B ‖ ab and B ‖ c at 2 and 4 K; (**b**) enlarged view of the central part of the hysteresis at 2 K (area indicated by the dashed line); (**c**) field dependence of J_c/J_c max ∝ ΔM in the B ‖ ab and B ‖ c at 2 K for EuRb−1144 single crystal.

4. Conclusions

In our paper, we have investigated single crystals of the stoichiometric iron-based superconductor $EuRbFe_4As_4$ grown by the self-flux method. Using high-resolution transmission electron microscopy, we observed an atomic structure of as-grown $EuRbFe_4As_4$ single crystals. HRTEM shows that crystals have two-dimensional intrinsic nanoscale inclusions that are found to be $RbFe_2As_2$ (122) phase with a volume fraction of ~5.6%. We establish the correlation between the structure defects in the single crystals of $EuRbFe_4As_4$ and SC properties. This nanoinclusions are not superconducting, so there is no second magnetization peak in the EuRb-1144 compound (as opposed to CaK-1144 in the B ‖ ab). We found the defects of the non-superconducting Rb-122 phase in the external magnetic field B ‖ ab have a two-dimensional layered structure. We assume the Rb-122 nanoinclusions in the $EuRbFe_4As_4$ compound act as 2D pinning centers.

Author Contributions: Conceptualization, A.Y.D., V.A.V. and K.S.P.; methodology, A.Y.D. and V.A.V.; validation A.Y.D., K.S.P. and V.A.V.; formal analysis, A.Y.D., V.A.V. and K.S.P.; investigation, A.Y.D., I.A.K., A.V.O., V.A.V. and K.S.P.; data curation, A.Y.D., I.A.K., A.V.O., V.A.V. and K.S.P.; writing—original draft preparation, A.Y.D. and V.A.V.; writing—review and editing A.Y.D., I.A.K., A.V.O., V.A.V. and K.S.P.; visualization, A.Y.D., I.A.K., A.V.O. and V.A.V.; supervision, V.A.V. and K.S.P. All authors have read and agreed to the published version of the manuscript.

Funding: This research was funded by the RUSSIAN SCIENCE FOUNDATION, project number 21-12-00394.

Institutional Review Board Statement: Not applicable.

Informed Consent Statement: Not applicable.

Data Availability Statement: The data that supports the findings in this study are available from the corresponding author upon reasonable request.

Acknowledgments: The work was performed using equipment of the Lebedev Physical Institute's Shared Facility Center. The authors are grateful to Vadim Amelichev "S-Innovations" LLC for operating XRD experiments.

Conflicts of Interest: The authors declare no conflict of interest.

References

1. Fertig, W.A.; Johnston, D.C.; DeLong, L.E.; McCallum, R.W.; Maple, M.B.; Matthias, B.T. Destruction of superconductivity at the onset of long-range magnetic order in the compound $ErRh_4B_4$. *Phys. Rev. Lett.* **1977**, *38*, 987–990. [CrossRef]
2. Bulaevskii, L.N.; Buzdin, A.I.; Kulić, M.L.; Panjukov, S.V. Coexistence of superconductivity and magnetism theoretical predictions and experimental results. *Adv. Phys.* **1985**, *34*, 175–261. [CrossRef]
3. Ishikawa, M.; Fischer, Ø. Destruction of superconductivity by magnetic ordering in $Ho_{1.2}Mo_6S_8$. *Solid State Commun.* **1977**, *23*, 37–39. [CrossRef]
4. Kamihara, Y.; Watanabe, T.; Hirano, M.; Hosono, H. Iron-based layered superconductor La $[O_{1-x}F_x]$ FeAs (x = 0.05–0.12) with T c = 26 K. *J. Am. Chem. Soc.* **2008**, *130*, 3296–3297. [CrossRef] [PubMed]
5. Cheng, P.; Shen, B.; Mu, G.; Zhu, X.; Han, F.; Zeng, B.; Wen, H.H. High-Tc superconductivity induced by doping rare-earth elements into CaFeAsF. *Europhys. Lett.* **2009**, *85*, 67003. [CrossRef]
6. Wu, G.; Xie, Y.L.; Chen, H.; Zhong, M.; Liu, R.H.; Shi, B.C.; Li, Q.J.; Wang, X.; Wu, T.; Yan, Y.J.; et al. Superconductivity at 56 K in samarium-doped SrFeAsF. *J. Phys. Condens. Matter* **2009**, *21*, 142203. [CrossRef]
7. Iyo, A.; Kawashima, K.; Kinjo, T.; Nishio, T.; Ishida, S.; Fujihisa, H.; Gotoh, Y.; Kihou, K.; Eisaki, H.; Yoshida, Y. New-structure-type Fe-based superconductors: $CaAFe_4As_4$ (A = K, Rb, Cs) and $SrAFe_4As_4$ (A = Rb, Cs). *J. Am. Chem. Soc.* **2016**, *138*, 3410–3415. [CrossRef]
8. Kawashima, K.; Ishida, S.; Fujihisa, H.; Gotoh, Y.; Kihou, K.; Yoshida, Y.; Eisaki, H.; Ogino, H.; Iyo, A. Superconductivity in a new 1144-type family of (La, Na) AFe_4As_4 (A = Rb or Cs). *J. Phys. Chem. Lett.* **2018**, *9*, 868–873. [CrossRef]
9. Huang, Q.; Qiu, Y.; Bao, W.; Green, M.A.; Lynn, J.W.; Gasparovic, Y.C.; Wu, T.; Wu, G.; Chen, X.H. Neutron-diffraction measurements of magnetic order and a structural transition in the parent $BaFe_2As_2$ compound of FeAs-based high-temperature superconductors. *Phys. Rev. Lett.* **2008**, *101*, 257003. [CrossRef]
10. Yuan, H.Q.; Singleton, J.; Balakirev, F.; Baily, S.A.; Chen, G.F.; Luo, J.L.; Wang, N.L. Nearly isotropic superconductivity in (Ba, K) Fe2As2. *Nature* **2009**, *457*, 565–568. [CrossRef]
11. Stolyarov, V.S.; Casano, A.; Belyanchikov, M.A.; Astrakhantseva, A.S.; Grebenchuk, S.Y.; Baranov, D.S.; Golovchanskiy, I.A.; Voloshenko, I.; Zhukova, E.S.; Gorshunov, B.P.; et al. Unique interplay between superconducting and ferromagnetic orders in $EuRbFe_4As_4$. *Phys. Rev. B* **2018**, *98*, 140506. [CrossRef]
12. Devizorova, Z.; Buzdin, A. Superconductivity-driven helical magnetic structure in $EuRbFe_4As_4$ ferromagnetic supercoductor. *Phys. Rev. B* **2019**, *100*, 104523. [CrossRef]
13. Stolyarov, V.S.; Pervakov, K.S.; Astrakhantseva, A.S.; Golovchanskiy, I.A.; Vyalikh, D.V.; Kim, T.K.; Eremeev, S.V.; Vlasenko, V.A.; Pudalov, V.M.; Golubov, A.A.; et al. Electronic Structures and Surface Reconstructions in Magnetic Superconductor RbEuFe4As4. *J. Phys. Chem. Lett.* **2020**, *11*, 9393–9399. [CrossRef]
14. Kim, T.K.; Pervakov, K.S.; Evtushinsky, D.V.; Jung, S.W.; Poelchen, G.; Kummer, K.; Vlasenko, V.A.; Sadakov, A.V.; Usoltsev, A.S.; Pudalov, V.M.; et al. Electronic structure and coexistence of superconductivity with magnetism in RbEuFe4As4. *Phys. Rev. B* **2021**, *103*, 174517. [CrossRef]
15. Bristow, M.; Knafo, W.; Reiss, P.; Meier, W.; Canfield, P.C.; Blundell, S.J.; Coldea, A.I. Competing pairing interactions responsible for the large upper critical field in a stoichiometric iron-based superconductor $CaKFe_4As_4$. *Phys. Rev. B* **2020**, *101*, 134502. [CrossRef]
16. Smylie, M.P.; Willa, K.; Bao, J.-K.; Ryan, K.; Islam, Z.; Claus, H.; Simsek, Y.; Diao, Z.; Rydh, A.; Koshelev, A.E.; et al. Anisotropic superconductivity and magnetism in single-crystal $RbEuFe_4As_4$. *Phys. Rev. B* **2018**, *98*, 104503. [CrossRef]
17. Song, B.Q.; Nguyen, M.C.; Wang, C.Z.; Ho, K.M. Stability of the 1144 phase in iron pnictides. *Phys. Rev. B* **2018**, *97*, 094105. [CrossRef]
18. Wang, Z.; Wu, S.; Ji, L.; Cao, G. Block-layer model for intergrowth structures. *Nano Res.* **2021**, *14*, 3629–3635. [CrossRef]
19. Liu, Y.B.; Liu, Y.; Cao, G. Iron-based magnetic superconductors $AEuFe_4As_4$ (A = Rb, Cs): Natural superconductor-ferromagnet hybrids. *J. Phys. Condens. Matter* **2021**, *34*, 093001. [CrossRef]
20. Uhoya, W.; Tsoi, G.; Vohra, Y.K.; McGuire, M.A.; Sefat, A.S.; Sales, B.C.; Mandrus, D.; Weir, S.T. Anomalous compressibility effects and superconductivity of EuFe2As2 under high pressures. *J. Phys. Condens. Matter* **2010**, *22*, 292202. [CrossRef]
21. Maiwald, J.; Gegenwart, P. Interplay of 4f and 3d moments in $EuFe_2As_2$ iron pnictides. *Phys. Status Solidi* **2017**, *254*, 1600150. [CrossRef]
22. Grinenko, V.; Drechsler, S.-L.; Abdel-Hafiez, M.; Aswartham, S.; Wolter, A.U.B.; Wurmehl, S.; Hess, C.; Nenkov, K.; Fuchs, G.; Efremov, D.V.; et al. Disordered magnetism in superconducting KFe_2As_2 single crystals. *Phys. Status Solidi* **2013**, *250*, 593–598. [CrossRef]
23. Hardy, F.; Böhmer, A.E.; Aoki, D.; Burger, P.; Wolf, T.; Schweiss, P.; Heid, R.; Adelmann, P.; Yao, Y.X.; Kotliar, G.; et al. Evidence of strong correlations and coherence-incoherence crossover in the iron pnictide superconductor KFe_2As_2. *Phys. Rev. Lett.* **2013**, *111*, 027002. [CrossRef]
24. Ishida, S.; Iyo, A.; Ogino, H.; Eisaki, H.; Takeshita, N.; Kawashima, K.; Yanagisawa, K.; Kobayashi, Y.; Kimoto, K.; Abe, H.; et al. Unique defect structure and advantageous vortex pinning properties in superconducting $CaKFe_4As_4$. *NPJ Quantum Mater.* **2019**, *4*, 27. [CrossRef]

25. Sugali, P.K.N.; Ishida, S.; Kimoto, K.; Yanagisawa, K.; Kamiya, Y.; Tsuchiya, Y.; Kawashima, K.; Yoshida, Y.; Iyo, A.; Eisaki, H.; et al. Intrinsic defect structures of polycrystalline $CaKFe_4As_4$ superconductors. *Phys. Chem. Chem. Phys.* **2021**, *23*, 19827–19833. [CrossRef]
26. Vlasenko, V.; Pervakov, K.; Gavrilkin, S. Vortex pinning and magnetic phase diagram of $EuRbF_{e4}As_4$ iron-based superconductor. *Supercond. Sci. Technol.* **2020**, *33*, 084009. [CrossRef]
27. Eltsev, Y.F.; Pervakov, K.S.; Vlasenko, V.A.; Gavrilkin, S.Y.E.; Khlybov, E.P.; Pudalov, V.M. Magnetic and transport properties of single crystals of Fe-based superconductors of the 122 family. *Uspekhi Fiz. Nauk.* **2014**, *184*, 897–902. [CrossRef]
28. Kim, T.; Pervakov, K.S.; Vlasenko, V.A.; Sadakov, A.V.; Usol'Tsev, A.; Evtushinsky, D.; Jung, S.; Poelchen, G.; Kummer, K.; Roditchev, D.; et al. Novel magnetic stoichiometric superconductor compound $EuRbFe_4As_4$. *Phys. Uspekhi* **2022**, *65*, 740–747. [CrossRef]
29. Bao, J.K.; Willa, K.; Smylie, M.P.; Chen, H.; Welp, U.; Chung, D.Y.; Kanatzidis, M.G. Single crystal growth and study of the ferromagnetic superconductor $RbEuFe_4As_4$. *Cryst. Growth Des.* **2018**, *18*, 3517–3523. [CrossRef]
30. Zhang, Z.; Wang, A.F.; Hong, X.C.; Zhang, J.; Pan, B.Y.; Pan, J.; Xu, Y.; Luo, X.G.; Chen, X.H.; Li, S.Y. Heat transport in $RbFe_2As_2$ single crystals: Evidence for nodal superconducting gap. *Phys. Rev. B* **2015**, *91*, 024502. [CrossRef]
31. Khim, S.; Aswartham, S.; Grinenko, V.; Efremov, D.; Blum, C.G.F.; Steckel, F.; Gruner, D.; Wolter, A.U.B.; Drechsler, S.-L.; Heß, C.; et al. A calorimetric investigation of $RbFe_2As_2$ single crystals. *Phys. Status Solidi* **2017**, *254*, 1600208. [CrossRef]
32. Jiang, S.; Luo, Y.; Ren, Z.; Zhu, Z.; Wang, C.; Xu, X.; Tao, Q.; Cao, G.; Xu, Z. Metamagnetic transition in $EuFe_2As_2$ single crystals. *New J. Phys.* **2009**, *11*, 025007. [CrossRef]
33. Bean, C.P. Magnetization of high-field superconductors. *Rev. Mod. Phys.* **1964**, *36*, 31–39. [CrossRef]